Technical Paper

ISSN 1997-1400 Int. J. Pavement Res. and Technol. 1(3):94-99

3D Microstructural Models for Asphalt Mixtures Using X-Ray Computed Tomography Images

Sanjeev Adhikari[1] and Zhanping You[2+]

Abstract: In this paper, aggregate orientation, aggregate gradation, sand mastic (a very fine sand-asphalt mixture) distribution, and air void distribution in the asphalt mixture were analyzed and modeled by capturing images using the X-ray Computed Tomography (CT) techniques. The mixture properties were predicted from X-ray CT images of the aggregate, mastic, and air voids. Moreover, the asphalt mixture images were utilized in modeling using the distinct element method approach for both two-dimensional (2D) and three-dimensional (3D) approaches. Three replicates of 3D distinct element model and six replicates of 2D distinct element model were simulated. 2D images were visualized by vertical orientation so that real distribution of air void levels could be captured. The mastic dynamic modulus and aggregate elastic modulus were determined and used as input parameters in the distinct element modeling. The strain responses of the asphalt mastic and mixture models under compressive load were monitored, and the dynamic moduli computed. The experimental measurements were compared with the 2D and 3D predictions. The 3D distinct element models were able to predict the asphalt mixture dynamic modulus. The 3D model's prediction is much better than that of 2D models. This outcome is a significant breakthrough in the modeling of asphalt mixture from 2D approach to 3D.

***Key words**: Asphalt mixture; Density index; Distinct element model; Dynamic modulus; Microstructural models; Sand mastic; Three dimensional; Two dimensional; X-ray computed tomography.*

Introduction

The internal structure of an asphalt mixture is influenced by the asphalt binder properties, aggregate properties, aggregate gradation and aggregate shape. This multiphase asphalt material has different properties from the original components of aggregate and mastic. The mastic (sand mixture) includes fine aggregate embedded in a matrix of asphalt binder. The particle size in the mastic is generally defined by a certain number (e.g. 2.36 or 0.6mm) depending upon the modeling and computing capacity. The dynamic modulus is an essential input parameter to the asphalt pavement mechanistic-empirical design [1]. Researchers have developed and applied distinct (discrete) element method in asphalt mixture modeling research in recent years [2-6].

The distinct element method (DEM) was developed by Cundall [7-10]. Collop et al. [11] applied a DEM to investigate the micromechanical behavior of idealized asphalt mixture. They stated that DEM can be used in asphalt mixtures to predict elastic, visco-elastic, and visco-plastic behavior. Abbas et al. [12] used the DEM in a sand mastic to simulate dynamic mechanical behavior. Buttlar and You [2] showed that the composite spherical model and the arbitrary phase geometry model, over- or under-predicted the stiffness of asphalt mixtures due to the inability of the models to predict the contribution of aggregate interlock to the response of asphalt mixture [4].

In this paper, asphalt mixture dynamic modulus was predicted by developing mechanics-based models which directly account for the complicated morphological study of asphalt concrete microstructure. The microstructure-based distinct element modeling approach used in this study includes the three dimensional (3D) and two dimensional (2D) models for asphalt mixtures. Micromechanical models can predict the fundamental material properties of an asphalt mixture based upon the properties of the individual constituents such as mastic and aggregate. The DEM is recognized as a good technique to determine the mechanical properties of the asphalt concrete microstructure [2-6].

Objectives

The objectives of this study are: 1) to develop 3D micromechanical distinct element models to simulate the asphalt mixture using X-ray Computed Tomography (CT) images; 2) to compare the modulus prediction from both 3D and 2D distinct element models with the lab measurements.

Scope

This study is focused on the application of a DEM to predict the dynamic modulus of the specimens using the heterogeneous microstructures visualized from X-ray CT images of the actual testing specimens. The laboratory tests of the asphalt mixtures and the sand mastic were conducted with the same equipment. The modeling approach was done with 2D and 3D DEM approaches taking into consideration of the actual air void distribution. The asphalt mixture modulus was predicted by using aggregate mastic stiffness.

Measurement of Dynamic Modulus

[1] Graduate Research Assistant and Ph.D. Candidate, Department of Civil and Environmental Engineering, Transportation Materials Research Center, Michigan Technological University, 1400 Townsend Drive, Houghton, Michigan 49931, USA.

[2] Donald and Rose Ann Tomasini Endowed Assistant Professor of Transportation Engineering, Department of Civil and Environmental Engineering, and Director of the Transportation Materials Research Center, Michigan Technological University, 1400 Townsend Drive, Houghton, Michigan, 49931, USA.

[+] Corresponding Author: E-mail zyou@mtu.edu

Note: Submitted December 15, 2007; Revised March 1, 2008; Accepted March 13, 2008.

Table 1. Aggregate Gradation of Asphalt Mixture and Sand Mastic.

Sieve Size (mm)	Percentage Passing by Weight	
	Asphalt Mixture	Sand Mastic
19	100.0	100.0
12.5	98.7	100.0
9.5	86.5	100.0
4.75	71.8	100.0
2.36	51.4	100.0
1.18	36.1	70.23
0.6	25.5	49.61
0.3	14.7	28.60
0.15	7.7	14.98
0.075	5.4	10.51

The dynamic modulus test was conducted according to the American Association of State Highway and Transportation Officials (AASHTO) standard TP62-03. A Superpave asphalt mixture with a 19mm of nominal maximum aggregate size was selected in this study. The asphalt was a Superpave Performance Grade (PG) 64-28 binder. The asphalt content of 5.6% was designed in the asphalt mixture. The asphalt mixture was compacted by a Superpave gyratory compactor to get a target air void level of 4.4%. Special designed sand mastic was used in this study, which is a very fine sand-asphalt mixture with a nominal maximum aggregate size of 2.36mm. The sand mastic was compacted on the cylindrical mold which had a height of 190mm and diameter of 76mm. The asphalt content of sand mastic was used by 10.3% by weight of the mixture and the air void levels were assumed to be zero due to the rich asphalt binder. Table 1 show the aggregate gradation used in this study. Stone cylinders were cored from the rock. The aggregate modulus was determined by the uniaxial compression test of the stone cylinder. For this study, an aggregate modulus of 55.5GPa was used in the models based upon the authors' experience with a large number of aggregates tested.

Dynamic (complex) modulus was measured for all three different specimens through uniaxial compressive tests. The dynamic modulus of the sand mastic and asphalt mixture were tested over a range of loading frequencies (0.1, 0.5, 1, 5, 10, and 25Hz) and temperatures (4, -6, and -18°C). The measurements of the asphalt mixture were compared with the dynamic modulus predictions to evaluate the distinct element modeling. The measurements of the sand mastic and aggregates were used as input parameters to the asphalt mixture models. The dynamic moduli of the asphalt mixture were used to assess the distinct element models.

Digital Image Processing of Asphalt Concrete

X-ray CT technique was used to provide geometric information to represent asphalt concrete for the DEM simulations, and to provide microstructure for the 3D quantification of particle kinematics in experiments in this study. X-ray CT is a nondestructive technique for visualizing features in the interior of solid objects to obtain digital information on their 3D geometry and properties. The detailed description of X-ray CT technology has been studied by various researchers such as Desrues et al. [13] and Raynaud et al. [14]. Part et al. [15] studied to show the homogeneity and isotropy during gyratory

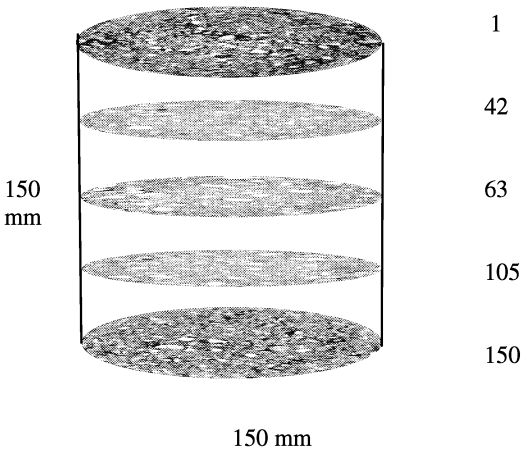

Fig. 1. Three-Dimensional Visualization of X-ray CT Image.

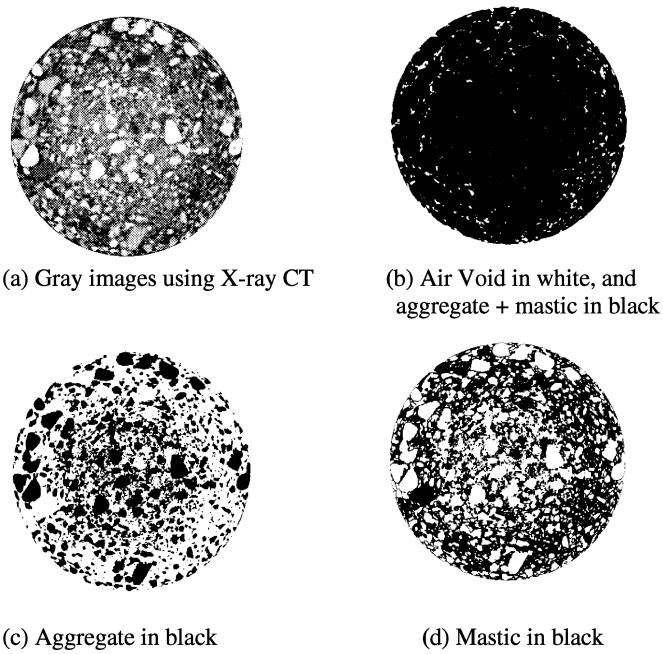

(a) Gray images using X-ray CT

(b) Air Void in white, and aggregate + mastic in black

(c) Aggregate in black

(d) Mastic in black

Fig. 2. Illustration of Gray Images Acquired by X-ray CT, Air Void, Aggregate, and Mastic Distribution in a 2D Space.

compaction in an asphalt concrete specimens using X-ray CT images. X-ray CT imaging is an advanced technique acquiring a stack of sectional images of material non-destructively.

Many researchers have used the X-ray tomography imaging technique to characterize the asphalt concrete in recent years [16-21]. The X-ray CT images were produced by the Federal Highway Administration (FHWA). A total of 150 images were analyzed for all specimens. Fig. 1 shows the 3D cylindrical asphalt specimen combinations of X-ray CT images. The height of the specimen is 150mm and the diameter is 150mm. The gray images acquired from an X-ray CT cannot be directly used in the data analysis. During the image processing, gray images were transferred into aggregate, mastic, and air void images according to a threshold segmenting of each element.

The gray image consists of density level of 256 that corresponds to different densities in the X-ray CT image. The air void level density

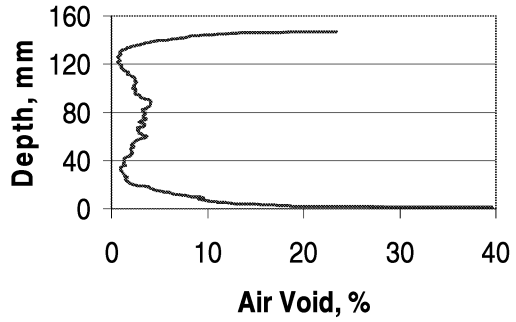

(a) Air Void Distribution of the Specimen

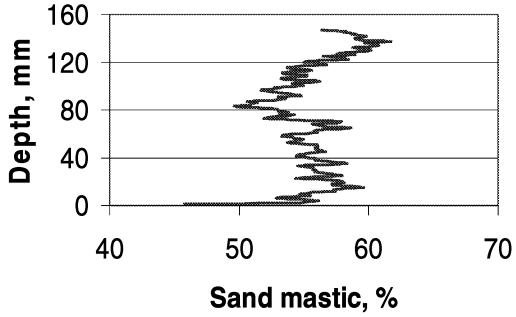

(b) Sand Mastic Distribution of the Specimen

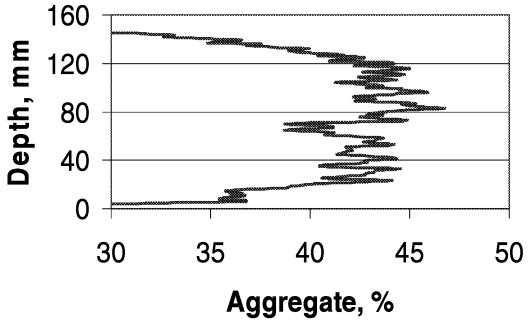

(c) Aggregate Distribution of the Specimen

Fig. 3. Air Void, Sand Mastic, and Aggregate Distribution of the Specimen.

index was chosen as 0-124, mastic density index chosen as 125-203, and the aggregate density index was chosen as 204-255.

The air void density index was determined by a measured air void level of 4.36%. Fig. 2 shows the air void domain, aggregate domain and mastic domain. The sand mastic is a combination of binder and aggregate which was finer than 2.36mm.

The 3D cylindrical asphalt specimen, which is a combination of X-ray CT images of the horizontal images along the depth, was analyzed. Fig. 3 shows distribution of air void, sand mastic, and aggregate according to depths of asphalt specimen. The air void distribution in the asphalt specimens follows a sigma shape. Larger air voids were gathered at the top and bottom of the specimens. The air void level decrease from the top to the middle and increase from the middle to the bottom. The sand mastic distribution in the asphalt specimens is almost uniform throughout the depth. The aggregate distribution increases from the top to the middle and decreases from the middle to the bottom.

Preparation of the Distinct Element Models

The asphalt mixture in this study is heterogeneous material of coarse aggregate, sand mastic, and air voids. The asphalt mixture microstructure was captured using X-ray tomography. The gray images of X-ray CT images were manipulated using image processing techniques and transferred into aggregate, mastic, and air void images according to a threshold segmenting of each element. The coordinate of aggregate, mastic, and air void was captured separately according to their threshold indices. The distinct element models used balls to represent the microstructure of the aggregate, mastic, and air void. The irregular shapes of aggregate, mastic, or air voids are composed of balls or spheres.

The 3D distinct element model was developed by a 3D rectangular prism shaped from the cylindrical specimen of asphalt concrete. For this study, three different rectangular prism shaped specimens were prepared. The 3D rectangular prism shaped specimen had used a length of 50mm, width of 50mm, and depth of 150mm in the DEM simulation. The radius of each sphere was 0.5mm. A total of 367,500 spheres were included in 3D DEM specimen without air voids. The air voids were around 4.36% (16,023 balls), which is comparable with the 4.4% air void in the compacted asphalt mixture. The aggregate volume was 40.78% (149,867 balls).

The 2D images were visualized from the vertical section of the asphalt specimen as shown in Fig. 4. The vertical images were captured from the stack of horizontal images by using an image processing technique. Two vertical images (at 22 and 44mm) were visualized on the 3D section using image processing as shown in Fig. 4(a). 2D sections were selected at the depth of 22, 44, 66, 88, 110, and 132mm on the 3D image. The 2D images from the vertical

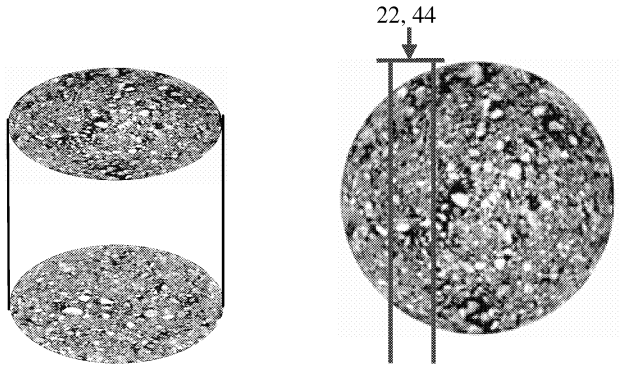

(a) Sectioning Pattern for Asphalt Concrete Specimens

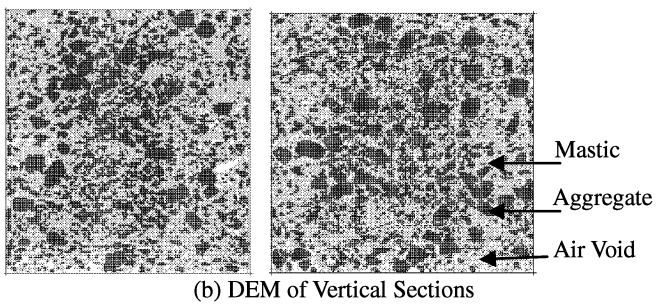

(b) DEM of Vertical Sections

Fig. 4. Illustration of Vertical Section from 3D Image.

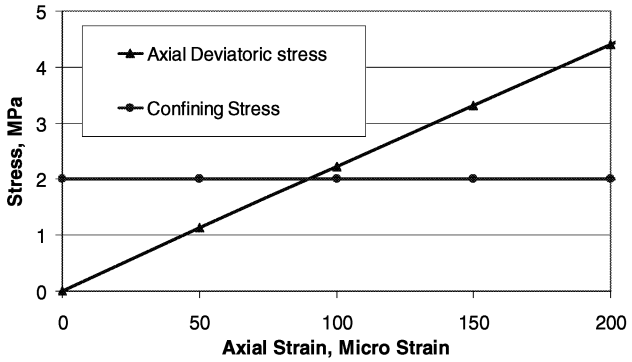

Fig. 5. Axial Deviator Stress and Confine Stress versus Axial Strain Using Triaxial Simulation of 3D DEM.

orientations were used for DEM simulation. Aggregate, mastic, and air void of 2D DEM are shown in Fig. 4(b). The 2D distinct element images showed inner 2D sections having higher air void levels than outer sections. The 2D and 3D distinct element models were constructed using face-centered packing spheres. The models were used to simulate the asphalt mixture dynamic moduli at different temperatures and frequencies.

Computation of Distinct Element Model

The dynamic modulus of the sand mastic and modulus of aggregate were measured and used in the distinct element models. The dynamic moduli of the asphalt mixture were used to assess the distinct element models. The application of the distinct element modeling approach was limited to the uniaxial/biaxial and triaxial compression test. The 2D and 3D microstructures of the asphalt mixture were obtained with the X-ray CT technique. The distinct element models were based on the microstructures of the mixtures.

The 2D and 3D DEM of the asphalt mixture was simulated by applying a compression test in a confined stress environment. The 2D and 3D specimens are computed using the biaxial test and triaxial compression test. A detailed discussion of the biaxial and the triaxial compression tests can be found in other literature [22]. An elastic relationship of the contact force and relative displacement between the elements was provided by the stiffness model.

In this paper, the dynamic moduli of asphalt mastic were measured in a uniaxial laboratory test program. The viscoelastic mastic dynamic modulus and elastic aggregate modulus were incorporated in microstructure based distinct element models to predict the mixture complex moduli. The corresponding principle [23] was applied by submitting viscoelastic mastic complex modulus to elastic simulation and linked the elastic and viscoelastic behavior through Laplace transformation.

The 2D and 3D DEM was loaded by the velocities on the top and bottom walls. The axial stress was computed from the average wall forces divided by appropriate area. The strains in the axial directions were calculated using the current model length divided by the original model length. The modulus was computed from the plot of the axial deviator stress versus axial strain. Axial deviator stress is defined as the difference between axial stress and confine stress. Fig. 5 shows the axial deviator and confining stress versus compressive strain using triaxial simulation of 3D DEM.

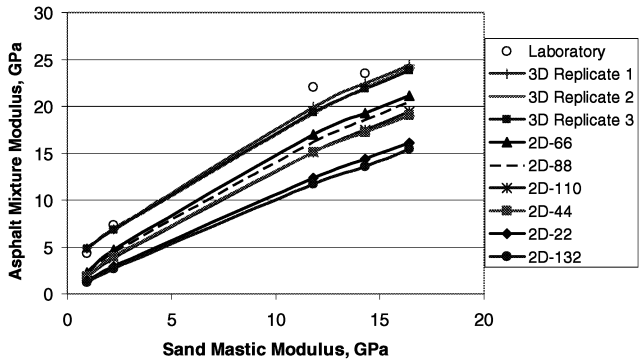

Fig. 6. Comparison of the Asphalt Mixture Modulus Using 3D DEM, 2D DEM, and Laboratory Asphalt Mixture from Mastic Modulus.

Simulation Results of the Distinct Element Models

In this section, the dynamic modulus simulation of the asphalt mixture using the 3D and 2D distinct element models is presented. The modulus simulation of the 3D DEM and 2D DEM results were compared with the laboratory measurements. Compressive test simulations were conducted using the 2D and 3D distinct element models. The air void levels of 3D cylindrical asphalt specimen (shown in Fig. 1) were compacted to 4.36%. The 2D and 3D DEM replicates were actually visualized from 3D cylindrical asphalt specimen. The air void levels, sand mastic volume, and aggregate volume varied in each replicates of 2D and 3D DEM. Fig. 6 shows the modulus prediction of the six 2D DEM, three 3D DEM, and laboratory asphalt mixtures. The dynamic modulus of the asphalt mastic of a loading frequency and a test temperature was used as input parameter to predict the dynamic modulus of a corresponding loading frequency and temperature in an asphalt mixture model. The 3D DEM prediction was very close to the laboratory measurement of asphalt mixture dynamic modulus. The average dynamic modulus of the six replicates for the 2D DEM model and the average dynamic modulus of the three replicates for the 3D model were compared with laboratory measurement. Fig. 7 shows a comparison of the dynamic modulus (E*) predictions using 2D DEM, 3D DEM, and laboratory measurements. When comparing the 2D and 3D models, it was found that 3D models yielded a better prediction for this mixture.

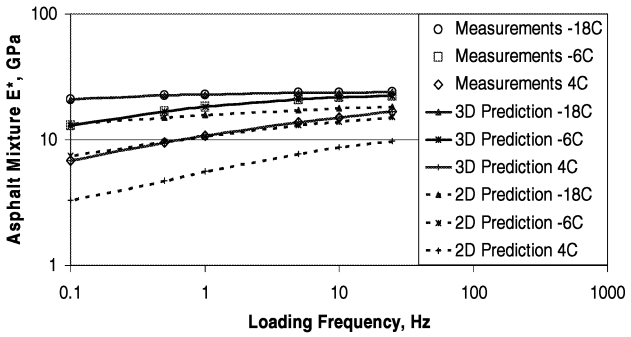

Fig. 7. Dynamic Modulus (E*) Prediction Using 2D and 3D DEM with Laboratory Measurement of the Asphalt Mixture.

The 3D modulus prediction is very close to the modulus obtained from laboratory measurement mixture for every temperature and frequency. The paired t-test was used to compare the mean difference between paired observations (predicted dynamic modulus and lab measured dynamic modulus). From the paired t-test results, it is found that the confidence interval of the 3D DEM prediction and the lab measurements is close to zero, which suggests there is no significant difference between the predicted dynamic modulus and lab measured dynamic modulus within a 95% confidence interval. The p-value at 0.005 suggests the 3D DEM predictions and the laboratory measurements are similar. The confidence interval is non-zero for a 3D DEM prediction and 2D DEM prediction, which means significant difference between them within a 95% interval. The confidence interval is non-zero for a 2D DEM prediction and lab measurements, which suggests a significant difference between them within a 95% confidence interval.

Summary and Conclusions

The X-ray CT images have been used for individual particle representation of the multiphase asphalt mixture. The computer automated procedures that integrates aspects of digital image analysis were developed to quantify the micro-structure of the asphalt mixture. The coordinates of the aggregate domain, sand mastic domain, and air voids domain in the asphalt mixture have been visualized by image processing. These coordinates were used for the 2D and 3D distinct element modeling. The modulus of the sand mastic and aggregate were used in the distinct element models to predict the dynamic modulus of the asphalt mixture. The 2D and 3D models were computed by using compressive loads to calculate the moduli of the specimen, which were derived from the stress-strain curve to reflect the specimen's macro response. The moduli of the 3D models were then compared with the experimental data. The 3D distinct element models were able to predict the asphalt mixture dynamic modulus.

In this paper, the dynamic modulus predictions obtained from the 2D and 3D DEM were compared, and it was found that the 3D DEM yielded higher modulus than the 2D DEM. Two dimensional models are difficult to describe aggregate's orientation and distribution in a three dimensional plane. The 3D asphalt mixture models describe a better aggregate interlock capability in the mixture, and therefore improve the predictions. The method provided in this paper is a significant breakthrough in asphalt mixture modeling from a 2D approach to 3D.

Acknowledgments

This material is based in part on work supported by the National Science Foundation under grant 0701264. Any opinions, findings, and conclusions or recommendations expressed in this material are those of the authors' and do not necessarily reflect the views of the National Science Foundation. The experimental work was completed in the Transportation Materials Research Center at Michigan Technological University, which maintains the AASHTO Materials Reference Laboratory (AMRL) accreditation on asphalt cement / cutback asphalt, hot mix asphalt, aggregates, and portland cement concrete. The authors appreciate Dr. M. Emin Kutay of the FHWA's Turner-Fairbank Highway Research Center for providing the X-ray tomography images.

References

1. American Association of State Highway and Transportation Officials (AASHTO), (2002). *AASHTO 2002 Design Guide - The Mechanistic-Empirical Pavement Design Guide (M-EPDG)*, Joint Task Force on Pavements and the National Cooperative Highway Research Program (NCHRP).
2. Buttlar, W.G. and You, Z., (2001). Discrete Element Modeling of Asphalt Concrete: A Micro-Fabric Approach, *Transportation Research Record,* No. 1757, pp. 111-118.
3. You, Z. and Buttlar, W.G., (2005). Application of Discrete Element Modeling Techniques to Predict the Complex Modulus of Asphalt–Aggregate Hollow Cylinders Subjected to Internal Pressure, *Transportation Research Record*, No. 1929, pp. 218-226.
4. You, Z. and Buttlar, W.G., (2006). Micromechanical Modeling Approach to Predict Compressive Dynamic Moduli of Asphalt Mixture Using the Distinct Element Method, *Transportation Research Record*, No. 1970, pp. 73-83.
5. You, Z., Adhikari, S., and Dai, Q., (2008). DEM Models of Idealized Asphalt Mixture, *ASCE Geotechnical Special Publication: Innovations in the Characterization, Modeling and Simulation of Pavements and Materials*, Proceedings of Symposium on Pavement Mechanics and Materials at the 18th ASCE Engineering Mechanics Division (EMD) Conference held in June 3-6 2007, Blacksburg, Virginia. Edited by Zhanping You, Ala R. Abbas, and Linbing Wang, published by American Society of Civil Engineers, Reston, Virginia, pp. 55-62.
6. You, Z., Adhikari, S., and Dai, Q., (2008). Two Dimensional and Three Dimensional Discrete Element Models for HMA, *ASCE Geotechnical Special Publication: Innovations in the Characterization, Modeling and Simulation of Pavements and Materials*, Proceedings of Symposium on Pavement Mechanics and Materials at the 18th ASCE Engineering Mechanics Division (EMD) Conference held in June 3-6 2007, Blacksburg, Virginia. Edited by Zhanping You, Ala R. Abbas, and Linbing Wang, published by American Society of Civil Engineers, Reston, Virginia, pp. 118-127.
7. Cundall, P.A., (2000). A Discontinuous Future for Numerical Modelling in Geomechanics, *Geotech. Eng*, **149**(1), pp. 41-47.
8. Cundall, P.A., (1990). Numerical Modeling of Jointed and Faulted Rock, *Proceedings of the International Conference on Mechanics of Jointed and Faulted Rock*, Vienna, Austria, pp. 11-18.
9. Cundall, P.A., (1987). Distinct Element Models of Rock and Soil Structure, Analytical and Computational Methods in Engineering Rock Mechanics, Chapter 4, Editor Brown, E.T., George Allen and Unwin, London, England, pp. 129-163.
10. Cundall, P.A., (1971). A Computer Model for Simulating Progressive Large Scale Movements in Blocky Rock Systems, *Proceedings of the Symposium of the International Society of*

Rock Mechanics, Vol. 1, Nancy, France, pp. 129-136.

11. Collop, A.C., McDowell, G.R., and Lee, Y., (2004). Use of the Distinct Element Method to Model the Deformation Behavior of an Idealized Asphalt Mixture, *International Journal Pavement Engineering*, Vol. 5, pp. 1-7.
12. Abbas, A., Masad, E., Papagiannakis, T., and Shenoy, A., (2005). Modeling Asphalt Mastic Stiffness Using Discrete Element Analysis and Micromechanics-Based Models, *International Journal of Pavement Engineering*, **6**(2), pp. 137-146.
13. Desrues, J., Chambon, R., Mokmi, M., and Mazerolle, F., (1996). Void Ratio Evolution inside Shear Bands in Triaxial Sand Specimens Studies by Computed Tomography, *Geotechnique*, **46**(3), pp. 529-546.
14. Raynaud, S., Fabre, D., and Mazerolle, F., (1989). Analysis of the Internal Structure of Rocks and Characterization of Mechanical Deformation by a Non-Destructive Method: X-ray Tomodensitometry, *Tectonophysics*, **159**(1-2), pp. 149-159.
15. Partl, M.N., Flisch, A., and Jönsson, M., (2003). Gyratory Compaction Analysis with Computer Tomography, *International Journal of Road Materials and Pavement Design,* **4**(4), pp. 401-422.
16. Shashidhar, N., (1999). X-ray Tomography of Asphalt Concrete, *Transportation Research Record*, No. 1681, pp. 186-192.
17. Braz, D., Lopes, R.T., and da Motta, L.M.G., (2000). Computed Tomography: an Evaluation of the Effect of Adding Polymer SBS to Asphaltic Mixtures Used in Paving, *Applied Radiation and Isotopes*, **53**(4), pp. 725-729.
18. Wang, L.B., Frost, J.D., and Shashidhar, N., (2001). Microstructure Study of Westrack Mixes from X-ray Tomography Images, *Transportation Research Board*, No. 1767, pp. 85-94.
19. Shi, B., Murakami, Y., Wu, Z., Chen, J., and Inyang, H., (1999). Monitoring of Internal Failure Evolution in Soils Using Computerization X-ray Tomography, *Engineering Geology*, **54**(3), pp. 321-328.
20. Masad, E., Jandhyala, V.K., Dasgupta, N., Somadevan, N., and Shashidhar, N., (2002). Characterization of Air Void Distribution in Asphalt Mixes Using X-Ray Computed Tomography, *Journal of Materials in Civil Engineering*, **14**(2), pp. 122-129.
21. Tian, L., Liu, Y., and Wang, B., (2007). 3D DEM Model and Digital Restructure Technique for Asphalt Mixture Simulation, *Journal of Changan University, Natural Science Edition*, **27**(4), pp. 23-26.
22. Itasca Consulting Group, (2004). PFC 3D Version 3.1 Minneapolis, Minnesota 55415, USA.
23. Flügge, W., (1975). Viscoelasticity, Berlin, Springer.